OPTIMIZATION OF LPB/SLM PROCESS AND MARAGING STEEL POWDERS FOR PLASTIC INJECTION MOULDS

Valentina Vicario[1], Daniele Miceli[2]
[1] MIMETE Srl, Via Padania 10, 20853 Biassono (MB), Italy
[2] RB Srl Via Gavioli 1, 41037 Mirandola (MO), Italy
Referring author: valentina.vicario@mimete.com

Abstract

Performances of plastic injection moulds heavily affect productivity and yields of high volume industries as packaging, cosmetics, … . RB is historically specialized in mould design and production and the introduction of a laser bed printer enlarged its possibilities especially in terms of optimization of cooling channels, more numerous and closer to the functional surface.
RB started working with commercial maraging and other steel powders: they observed some differences among producers and grades and started questioning about the relationship between powders and printing parameters. The necessary metallurgical competences and laboratory equipment have been found in MIMETE, the new Italian metal powders producer. The two companies are working together on a long-term European project aiming at the development of new optimized powders and LPB/SLM process parameters to:
1) maximize productivity
2) control roundness and roughness of cooling channels
3) maximize powder life
4) reduce tendency to cracking
5) increase thermal fatigue properties.

Keywords

Maraging metal powders; powder bed selective laser melting (LPB/SLM); plastic injection moulds

1. Introduction

This paper describes the initial activities performed to define the state of the art of LPB/SLM applied to maraging steel powders. A comparative analysis of commercial powder properties and samples obtained with a DOE including multiple combination of process parameters is reported. Moreover a characterization of powders after multiple printing cycles has been run to evaluate the aging phenomena and define if powder can be reused and how many times.
These initial results already indicate a possible set of powder properties and more influencing machine parameters that optimize density of final product. The experimental work will be completed with further powders and deeper investigations of the effect of single parameters in order to finalize a complete optimized production chain for plastic injection moulds.

2. Material and experimental method

In order to understand the effect of starting material on components printed by LPB/SLM, different commercial maraging M300 powders were tested as starting point.

Below a table of powder characteristics, as per supplier certificates.

Supplier	L	S
Nominal PSD d10 [µm]	17	17
Nominal PSD d50 [µm]	29	36
Nominal PSD d90 [µm]	47	65
Hall flow rate [s/50g]	15	-
Apparent density [g/cm3]	4	-

Table 1: powder data as reported in supplier certificate

MIMETE carried out a complete characterization of powders in its fully equipped laboratory. Powders were analysed both in the delivery condition and in one case also after printing (samples: E2 = after 2 jobs; E10 = after 10 jobs), in order to crosscheck suppliers certificates and evaluate how powder properties change after usage.

Sample preparation

As reported in different works [1] and [2] sample handling is crucial for good results: for this reason powder was taken from commercial packaging opened under inert atmosphere, blended and quarted prior sample taking.

Practice for chemical analysis

Oxygen and Nitrogen content on the powder was determined using an analyzer based on inert gas fusion principle in a graphite crucible at high temperature, according to ASTM standard [3].

Carbon and sulphur content on the powder was determined using an analyser based on induction furnace melting and gas detection in IR cells, according to ASTM standard [3].

Chemical analysis on other elements was carried out using ICP-OES, according to ASTM standards [4] and [5].

Practice for technological properties

The following physical properties were tested in MIMETE Laboratory: Hall flowability, apparent density, tap density; all the tests were carried out in accordance with ASTM standards [6], [7] and [8].

In addition, the powders were screened using scanning electron microscope both at low and high magnification, in order to verify by morphological inspection the presence of surface oxidation applying MIMETE's internal procedure, based on morphology/density and percentage of coverage of oxide layer on particle surface. After cold mounting a microstructural analysis was also carried out using a light optical microscope both on polished and etched samples.

3. As supplied powder characterization results

Chemical analysis

Supplier Element [%]	L	S
Al	0.12	0.11
Co	9.3	9.3
Cr	**0.05**	**0.18**
Cu	-	0.03
Fe	bal	bal
Mn	0.01	0.06
Mo	4.9	5.0
Ni	**18.5**	**18.1**
P	0.004	0.007
Si	0.03	0.07
Ti	**1.13**	**0.81**
C	0.001	0.010
S	0.004	0.003
O [ppm]	**261**	**384**
N [ppm]	271	**363**

Table 2: chemical composition of tested powders

As visible, all the powders analysed shown a similar chemical composition regarding major elements, except for meaningful differences on Ti and some singularities on Cr, Ni and nitrogen. Note that also oxygen levels, which is critical for AM process, are different.

Technological properties

Supplier	L	S
PSD d10 [µm]	16.9	17.5
PSD d50 [µm]	**28.9**	**36.4**
PSD d90 [µm]	**47.2**	**63.2**
Apparent density	4.1	4.3
Tap density	5.0	5.1
Hausner ratio	1.22	1.19
Hall flow s/50g (as supplied)	16	NO flow
Hall flow s/50g (after drying 180°C for 2h)	-	13

Table 3: technological properties of tested powders

Tested powders show different PSD distribution: sample S is coarser than sample L, even if the smallest particles are similar in size.

As visible sample S show a bad flow behavior in as received condition, but after after drying the flowability is similar to the other powders, probably indicating some adsorbed humidity in the packaging.
Apparent and tap values are similar.

Scanning electron microscopy

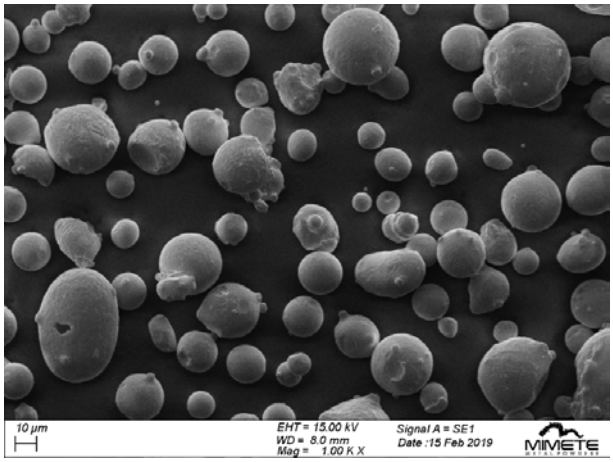

Supplier L

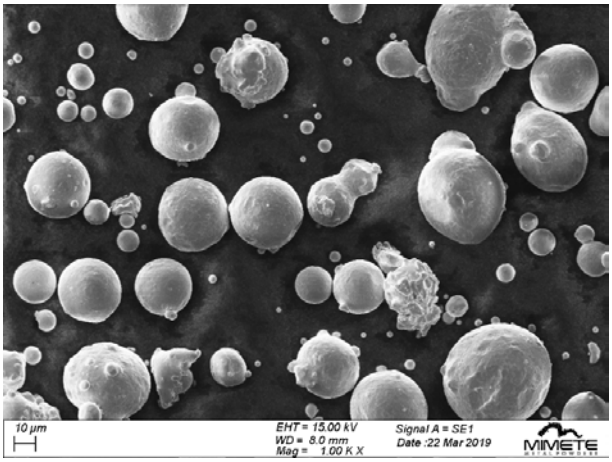

Supplier S

Figure 1 (a-b): pictures of tested powders, SE

As visible in low magnification analysis (1000X) the powders are comparable: they have a quite spherical ratio and limited satellites and clusters. These results have no relationship with flowability evidences.

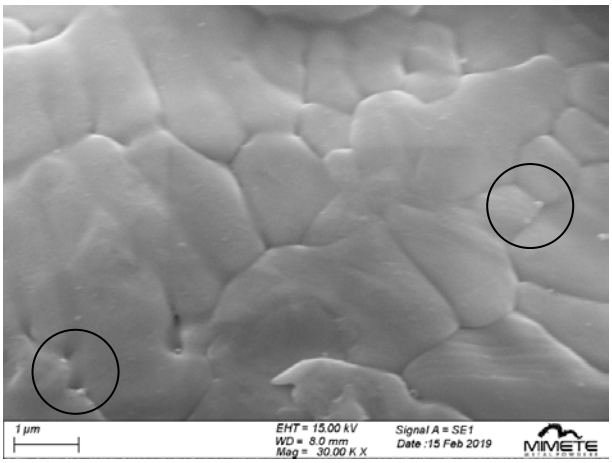

Supplier L

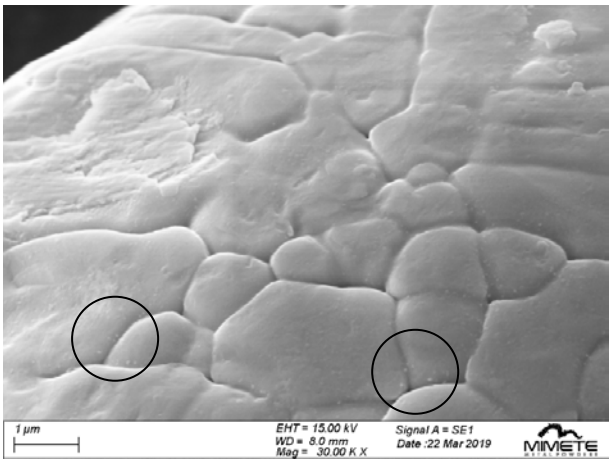

Supplier S

Figure 2 (a-b): surface texture of tested powders, SE

Both samples S and L show a very light oxidation, visible as small points on the surface (see round circles). These results have no relationship with flowability evidences.

Light optical microscope

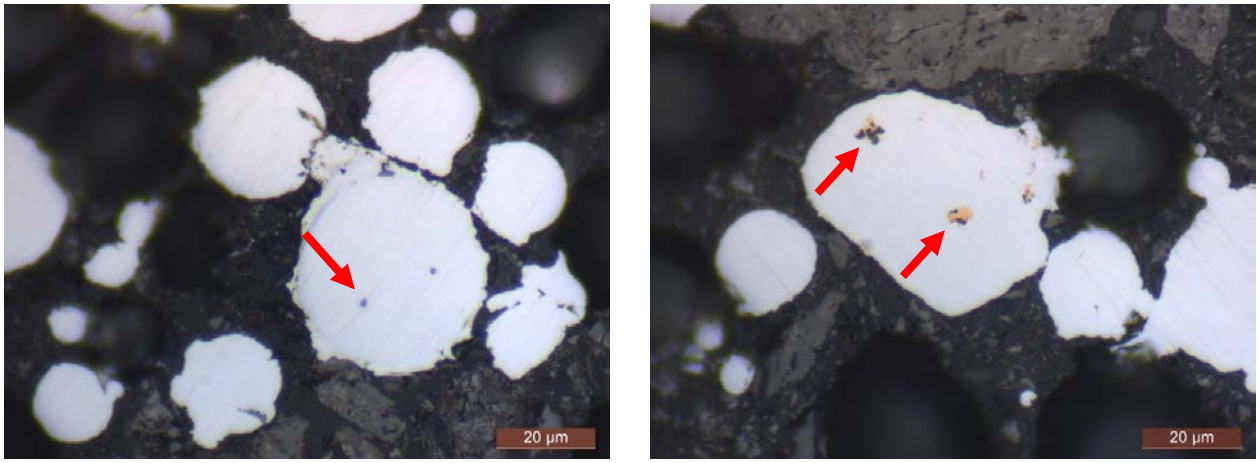

Supplier L *Supplier S*

Figure 3 (a-b): micro-inclusions of tested powders, LOM

On representative pictures of just polished samples L and S some nitrides are clearly visible, more frequent on sample S (maybe justified by higher nitrogen content).
On etched samples a martensitic mostly equiaxial solidification structure, typical of fast cooling during atomization, is present.

4. LPB/SLM trials

DOE design

In order to evaluate how different chemical-physical powder properties interact with different laser parameters, a 2-level-factorial design of experiment, with 2^{5-1} experiments and 3 center points, was selected. This approach is very useful to identify which are the most important factors that affect process quality. After the screening phase, it is possible to fine-tune the DOE excluding ineffective parameters.

Statistical analysis on responses of DOE implies the choice of effective parameters (input factor or their combinations) that correlate the resulting data in a significant model. The Pareto chart was used as method to analyze test results, applying Bonferroni limit as coefficient indicating the likelihood of correlation between the output and the input [10].

DOE parameters

RB printed cubic specimens (10 x 10 x 10 mm) using a EOSINT M280, a Selective Laser Melting EOS machine equipped with a 400 W Ytterbium fibre laser.

For each type of powder (L and S) 20 different specimens have been printed according to 19 different experiments plus an additional sample built with EOS Standard parameter. Stripe width (10.00 mm), layer thickness (40 µm), plate temperature (40°C) and inert gas (nitrogen) are kept constant. All other editable parameters are varied in a defined range as follows:

Run	A: Hatch Distance [mm]	B: Speed [mm/s]	C: Power [W]	D: Beam Offset [mm]	E: Stripes overlap [mm]
1	0.08	1020	320	-0.045	0.06
2	0.08	1020	250	-0.065	0.06
3	0.08	900	320	-0.045	0.1
4	0.14	900	250	-0.045	0.1
5 (central)	**0.11**	**960**	**285**	**-0.055**	**0.08**
6	0.08	1020	250	-0.045	0.1
7	0.14	1020	250	-0.065	0.1
8	0.14	900	320	-0.045	0.06
9	0.14	900	320	-0.065	0.1
10	0.14	900	250	-0.065	0.06
11	0.08	900	250	-0.065	0.1
12	0.11	960	285	-0.055	0.08
13	0.08	1020	320	-0.065	0.1
14	0.11	960	285	-0.055	0.08
15	0.08	900	320	-0.065	0.06
16	0.14	1020	320	-0.065	0.06
17	0.14	1020	320	-0.045	0.1
18	0.14	1020	250	-0.045	0.06
19	0.08	900	250	-0.045	0.06
20	**EOS STD PARAMETERS**				

Table 4: matrix of parameters applied for different tests of the DOE

Unfortunately, EOS STANDARD PARAMETERS (set # 20) are not kwon (closed condition) but we can assume that they are close to EOS “central” Editable parameters (set # 5).

The response parameter to evaluate is density, determined by hydrodensitometry.

L Powder: Analysis of DOE results

Fig. 4 shows that A (distance) and C (power) parameters exceed the Bonferroni Limit (red line), as they have the most significant impact on density. On the other hand, B parameter (Scan Speed) shows a slight influence on output, but the range of variation seems not so extended to cause a considerable effect. Remaining parameters (Beam offset and stripes overlap) and the combination of the five input show even less correlation.

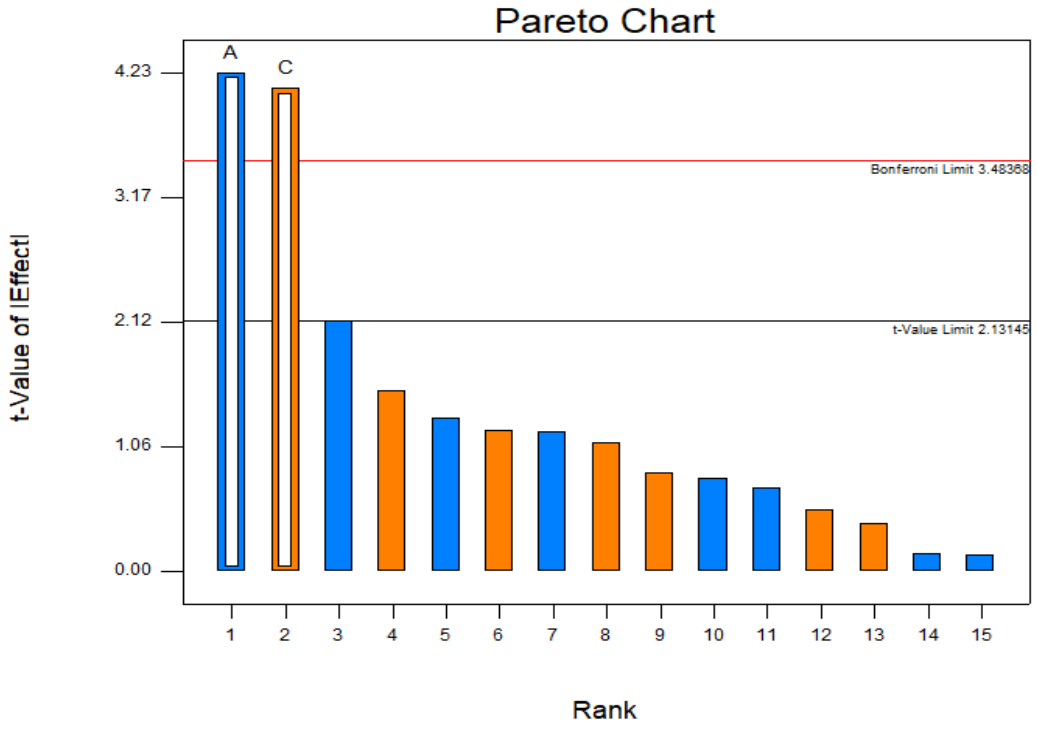

Figure 4: Pareto chart summarizing experimental results of DOE on L powder

The contour plot of the density as function of two selected parameters, distance and power, shows a linear correlation with both. As predictable, density decreases with hatch distance and increases with power.

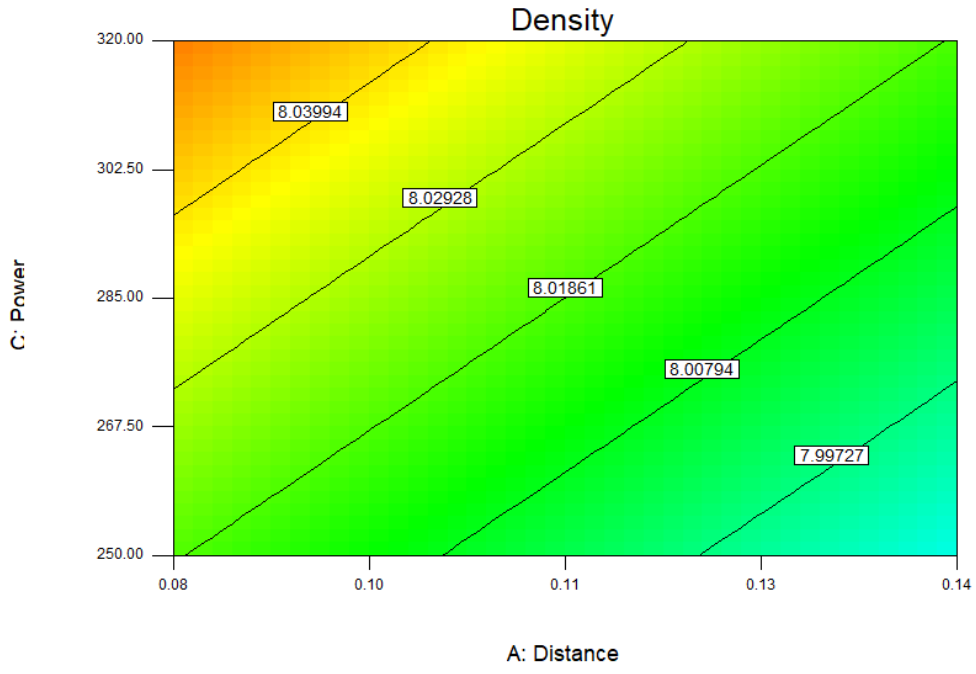

Figure 5: Correlation between most influencing parameters and density of L powder

S Powder: Analysis of DOE results

The S powder shows the same impact of input A and C on density value as previous model. It is interesting to notice how the combination of D*E acquires more importance than B parameter (even if it does not reach the Bonferroni limit). It could be due to the finer fraction of the powder that is affected by local overheating due to combination of high thermal input.

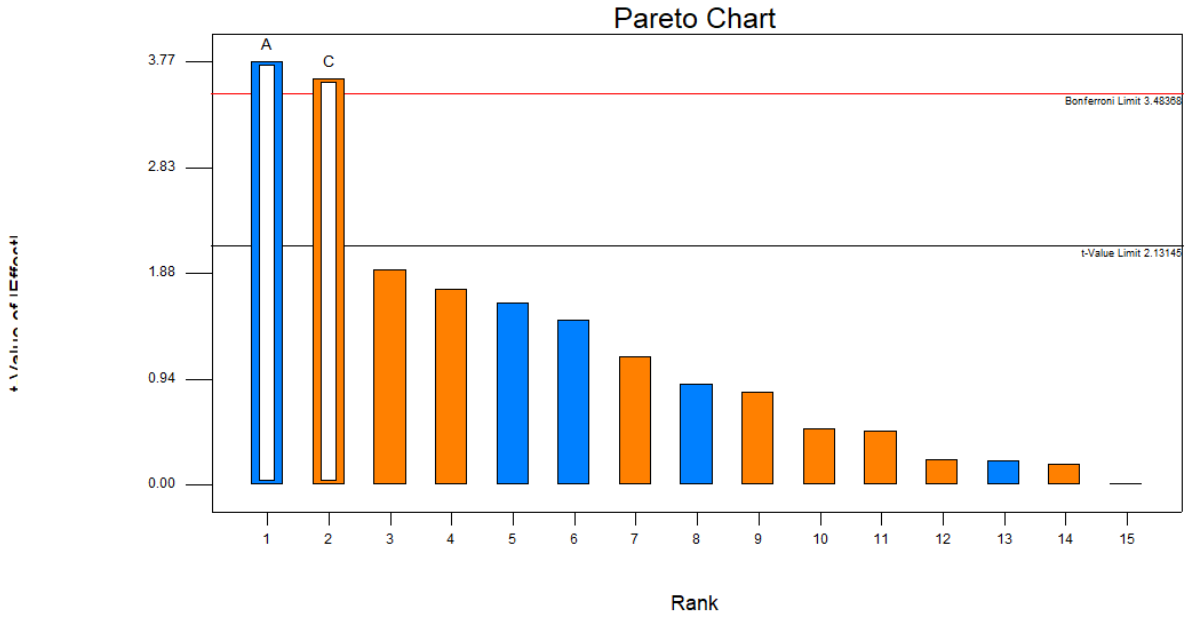

Figure 6: Pareto chart summarizing experimental results of DOE on S powder

The contour chart shows results similar to those obtained with L powder, but with a higher maximum value of absolute density due to alloy composition itself.

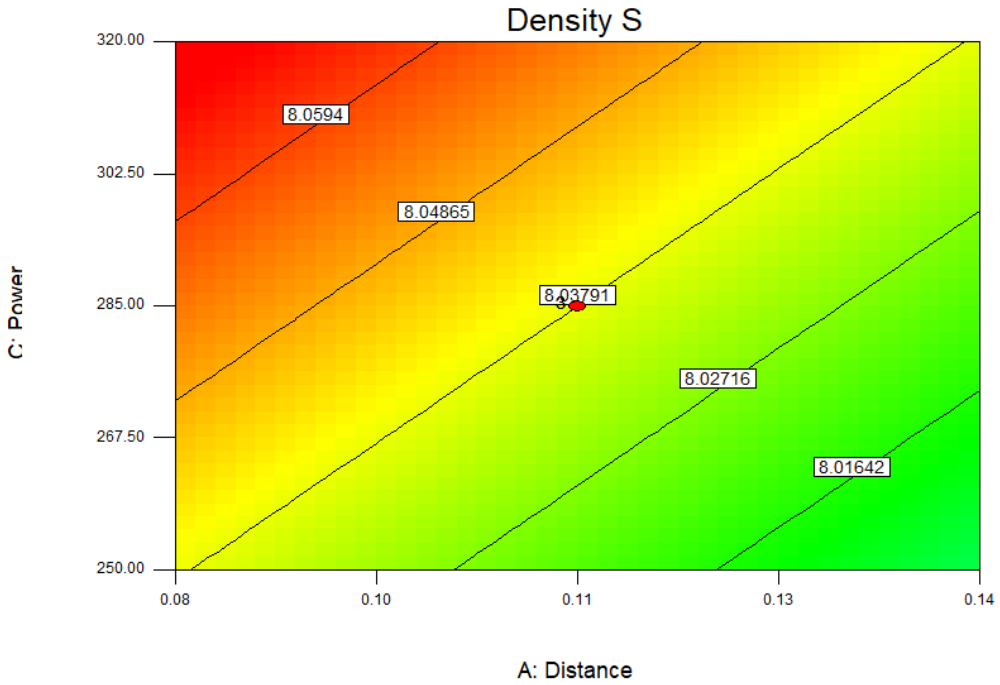

Figure 7: Correlation between most influencing parameters and density of S powder

Comparison of powders

Density of printed samples is evaluated as a function of energy density [J/mm^3], defined as:

$$E_d = \frac{P_{eff}}{v_s \cdot h \cdot d} \quad [9]$$

where E_d is the energy density in J/mm^3, P_{eff} is the effective laser power (W), v_s is the laser scan speed (mm/s), h is the hatch distance (mm) and d is the thickness of the layer (mm). This equation does not consider other important factors such exposure strategy, laser offsets at corners, laser spot size, stripes overlap, ... [10]

In order to compensate higher bulk density of S powder (due to lower content of light elements and higher content of heavy elements), to compare the two powders we related the measured density values with the maximum value measured above all the samples. Even then, S powder shows a better relative density for each experiment. For both Powder, the EOS Standard Parameters show a relative density among the highest measured.

Run	**Energy density [J/mm^3]**	**L Density [g/cm^3]**	**S Density [g/cm^3]**
1	98.04	99,76%	99,92%
2	76.59	99,46%	99,87%
3	111.11	99,58%	99,95%
4	49.60	99,14%	99,37%
5 (central)	67.47	99,46%	99,81%
6	76.59	99,47%	99,71%
7	43.77	98,65%	98,66%
8	63.49	99,62%	99,77%
9	63.49	99,49%	99,69%
10	49.60	99,33%	99,58%
11	86.81	99,60%	99,66%
12	67.47	99,50%	99,84%
13	98.04	99,68%	99,90%
14	67.47	99,47%	99,76%
15	111.11	100,00%	100,00%
16	56.02	99,50%	99,66%
17	56.02	99,38%	99,78%
18	43.77	98,72%	98,97%
19	86.81	99,50%	99,72%
20	**EOS STD**	99,78%	99,90%

Table 5: matrix of density measured for different tests of the DOE

During the building of the samples the ones with higher energy density show intense overheating with the appearance of oxidized phase, nonetheless the samples reach a high value of density except for the n. 3 of L powder. A metallographic inspection will be run to check that no internal defects are present.

It is interesting to point out how the two powders show a very evident difference in density in the center part of the charts, for "average" energies from 65 to 75 J/mm^3, which are the typical values for standard printing. It is possible to assume that in this region different powders require a fine tuning of process parameters to reach optimal density.

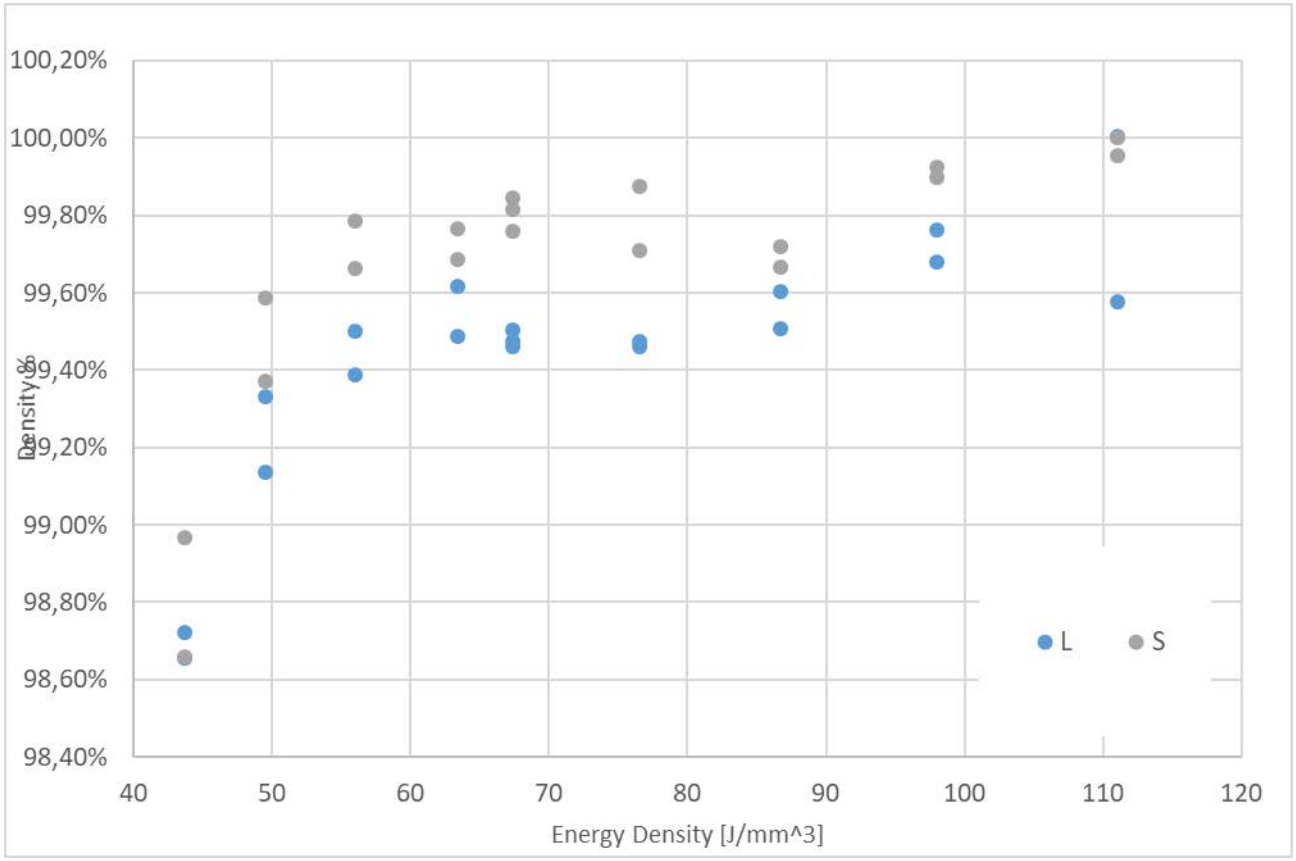

Figure 8: density measured for different tests of the DOE

5. After use powder characterization results

Chemical analysis

Supplier Element [%]	E	E2	E10
N° of jobs	0	2	10
O [ppm]	358	610	~ 1600
N [ppm]	275	274	278

Table 6: technological properties of used powder

Oxygen pick-up is clearly visible just after 10 jobs on +63 µm powder (fraction removed by sieves used to recover powder for new jobs). The powder analysed after 2 jobs shows very lower value of oxygen, probably also due to -63 µm size.

Technological properties

Supplier	E	E2	E10
N° of jobs	0	2	10
Nominal PSD	*< 63 µm*	*< 63 µm*	*> 63 µm*
PSD d10 [µm]	16.9	18.9	61
PSD d50 [µm]	34.8	35.0	98
PSD d90 [µm]	60.7	60.9	155
Apparent density	4.3	4.6	-
Tap density	5.1	-	-

Table 7: technological properties of used powder

Technological properties comply with expectations.

Scanning electron microscopy

After 2 jobs some clusters and agglomerates are yet present on the recycled fraction, as due to their dimension are not easily removable by sieving after each job.

The presence of surface oxidation is evident after 10 jobs on but is already visible 2 jobs, suggesting that printing parameters (especially chamber atmosphere) are causing a very fast aging of powders, limiting their life and possibility to be reused.

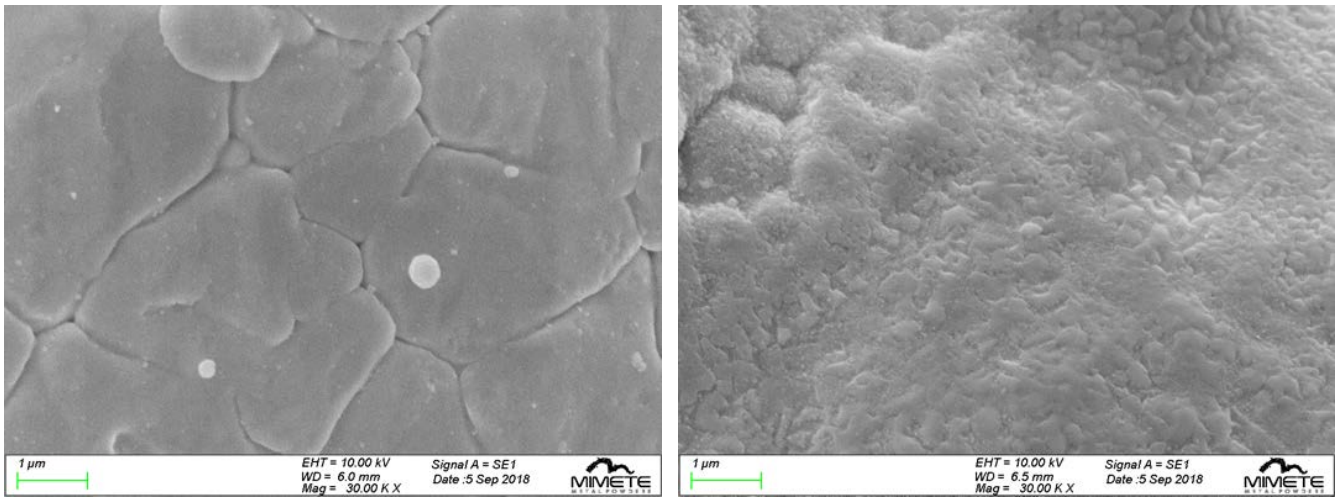

Sample E2 *Sample E10*

Figure 9 (a-b): surface texture of tested powders, SE, magnification 30000X

6. Conclusions

- The namely equivalent powders available on the market show different properties, both in terms of chemical analysis, particle size distribution, morphology. DOE results show that this brings to some differences in final density of printed samples applying the same parameters, so theoretically every powder should require an optimization of the PBD/SLM process
- For every combination of process parameters, the powder with smaller particles, lower Ti and Ni and higher Cr and N_2 brings to higher density of printed parts. Further investigation is need to separate the effect of each of these variables.

- Hatch distance and laser power are the process parameters that have the most significant impact on density. It is possible that scan speed effect is underestimated due to too limited tested range
- Beam offset and stripes overlap have a meaningful effect only with finer particles, probably more sensible to geometrical parameters due to higher energy concentration
- Increase of O_2 content and surface oxidation is already visible on powders after 2 jobs, suggesting that printing parameters (especially chamber atmosphere) are causing a very fast aging of powders, limiting their life and possibility to be reused.

7. References

[1] ASTM, B215-15: Standard Practices for Sampling Metal Powders. (2015)
[2] Cochran, W.G. 1977. Sampling Techniques, Third Edition. Wiley, New York.
[3] ASTM, E1019 – 18 Standard Test Methods for Determination of Carbon, Sulfur, Nitrogen, and Oxygen in Steel, Iron, Nickel, and Cobalt Alloys by Various Combustion and Inert Gas Fusion Techniques. (2018)
[4] ASTM, E1479-16: Standard Practice for Describing and Specifying Inductively Coupled Plasma Atomic Emission Spectrometers. (2016)
[5] ASTM, E2594-09 Standard Test Method for Analysis of Nickel Alloys by Inductively Coupled Plasma Atomic Emission Spectrometry (Performance-Based Method). (2014)
[6] ASTM, B213-17: Standard Test Methods for Flow Rate of Metal Powders Using the Hall Flowmeter Funnel. (2017)
[7] ASTM, B212-17 Standard Test Method for Apparent Density of Free-Flowing Metal Powders Using the Hall Flowmeter Funnel. (2017)
[8] ASTM, B527 – 15 Standard Test Method for Tap Density of Metal Powders and Compounds. (2015)
[9] Carter LN. Wang X. Read N. et al. Process optimization of selective laser melting using energy density model for nickel based superalloys. Mater Sci Tech. 2015;32:1–5
[10] K. G. Prashanth. S. Scudino. T. Maity. J. Das & J. Eckert (2017) Is the energy density a reliable parameter for materials synthesis by selective laser melting? Materials Research Letters. 5:6. 386-390. DOI: 10.1080/21663831.2017.1299808